In-Situ Synthesis of MXene@Iron Oxide Nanoparticle Composites *via* Pulsed Laser Ablation in Liquid applied for electrochemical H_2O_2 reduction

Lenka Lorencová[a, b], Eva Noskovičová[b, c], Monika Jerigová[b, c], Monika Stupavská[d], Ľubomír Orovčík[e], Lucia Kopčanová[e], Peter Kasák[f], Andrej Vikartovský[a, g], Dušan Lorenc[c, h], Khaled A. Mahmoud[i], Ján Tkáč[a]

[a]Institute of Chemistry, Slovak Academy of Sciences, Dubravska cesta 5807/9, 845 38, Bratislava,
Slovak Republic

[b]Department of Physical Chemistry, Faculty of Natural Sciences, Comenius University, Mlynska dolina,
842 15, Bratislava, Slovak Republic

[c]International Laser Centre-Slovak Centre of Scientific and Technical Information, Ilkovicova 3, 841 04, Bratislava, Slovak Republic

[d]Department of Plasma Physics and Technology, CEPLANT—R&D Centre for Plasma and Nanotechnology Surface Modifications, Faculty of Science, Masaryk University, Kotlářská 267/2, 602 00 Brno,
Czech Republic

[e]Institute of Materials and Machine Mechanics, Dubravska cesta 9/6319, 845 13, Bratislava,
Slovak Republic

[f]Center for Advanced Materials, Qatar University, P.O. Box 2713, Doha, Qatar

[g]Department of Analytical Chemistry, Faculty of Natural Sciences, Comenius University, Ilkovicova 6,
842 15 Bratislava, Slovak Republic

[h]RCQI, Institute of Physics, Slovak Academy of Sciences, Dubravska cesta 9, 841 04, Bratislava,
Slovak Republic

[i] Qatar Environment and Energy Research Institute, Hamad Bin Khalifa University, P.O. Box 34110, Doha, Qatar

NP size distribution

The NP diameters were evaluated by applying the Hough circular transform to the acquired SEM images. Respective images of MXenes with FeNPs are shown in **Fig. S1a**, **S2a** and **S3a** with the actual position and sizes of the NPs marked by coloured circles. A corresponding histogram providing the NPs diameter distribution is depicted in **Fig. S1b**, **S2b** and **S3b**. A relatively broad distribution function is typical of LAL.

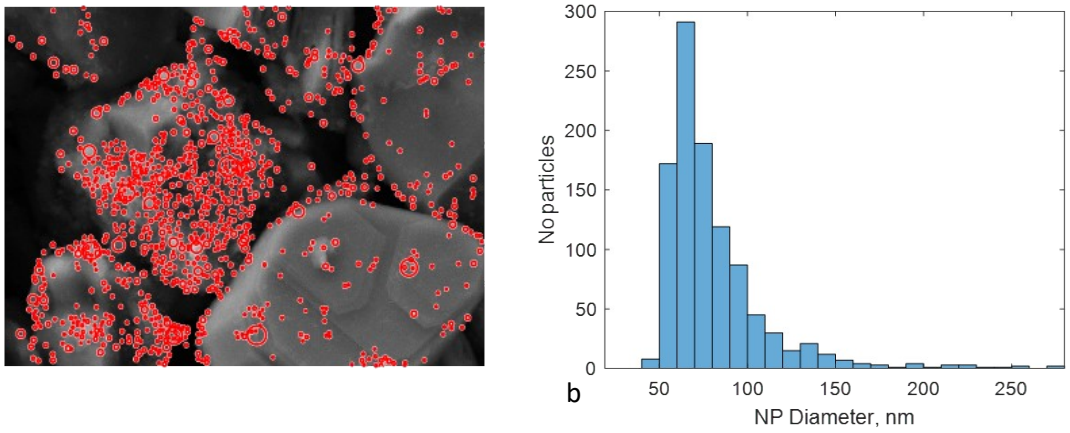

Fig. S1: FeNPs decorated $Ti_3C_2T_x$ MXene with the resolved positions of NPs marked by circles (**a**) and the corresponding histogram of NP diameters (**b**).

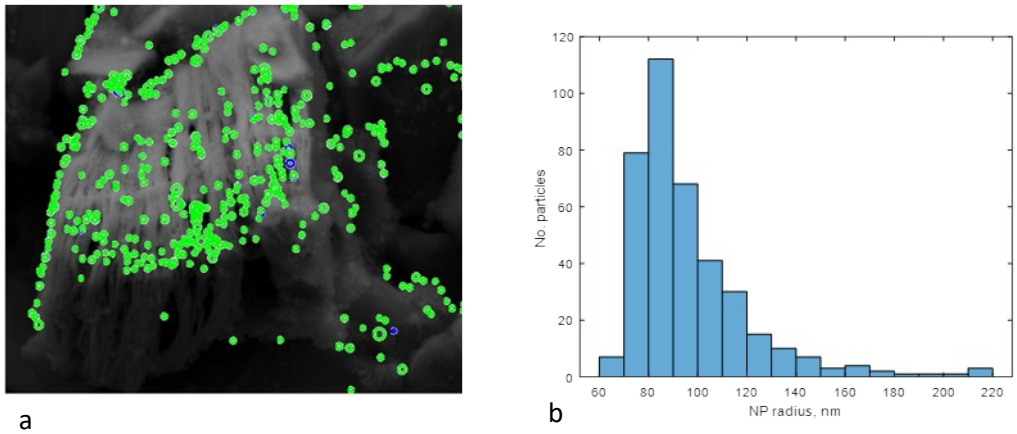

Fig. S2: FeNPs decorated $Nb_4C_3T_x$ MXene with the resolved positions of NPs marked by circles (**a**) and the corresponding histogram of NP diameters (**b**).

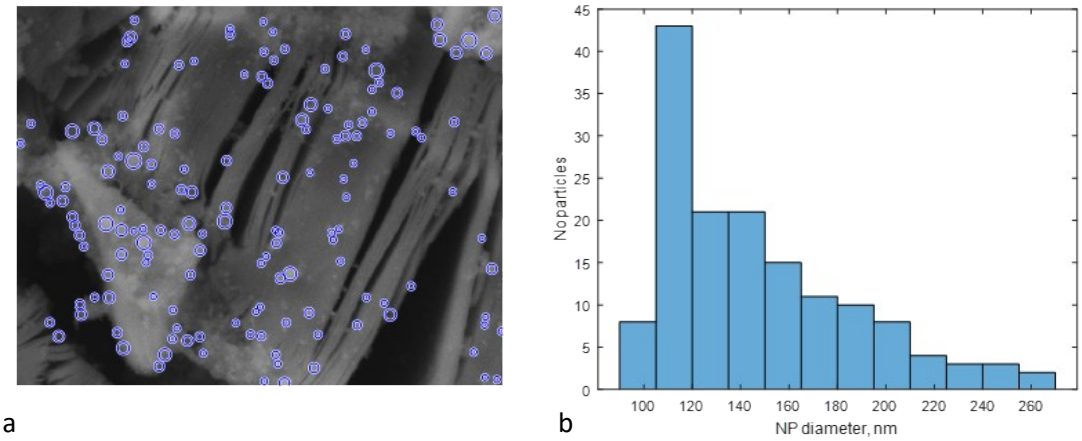

Fig. S3: FeNPs decorated Nb_2CT_x MXene with the resolved positions of NPs marked by circles (**a**) and the corresponding histogram of NP diameters (**b**).

Secondary Ion Mass Spectrometry (SIMS) Analysis

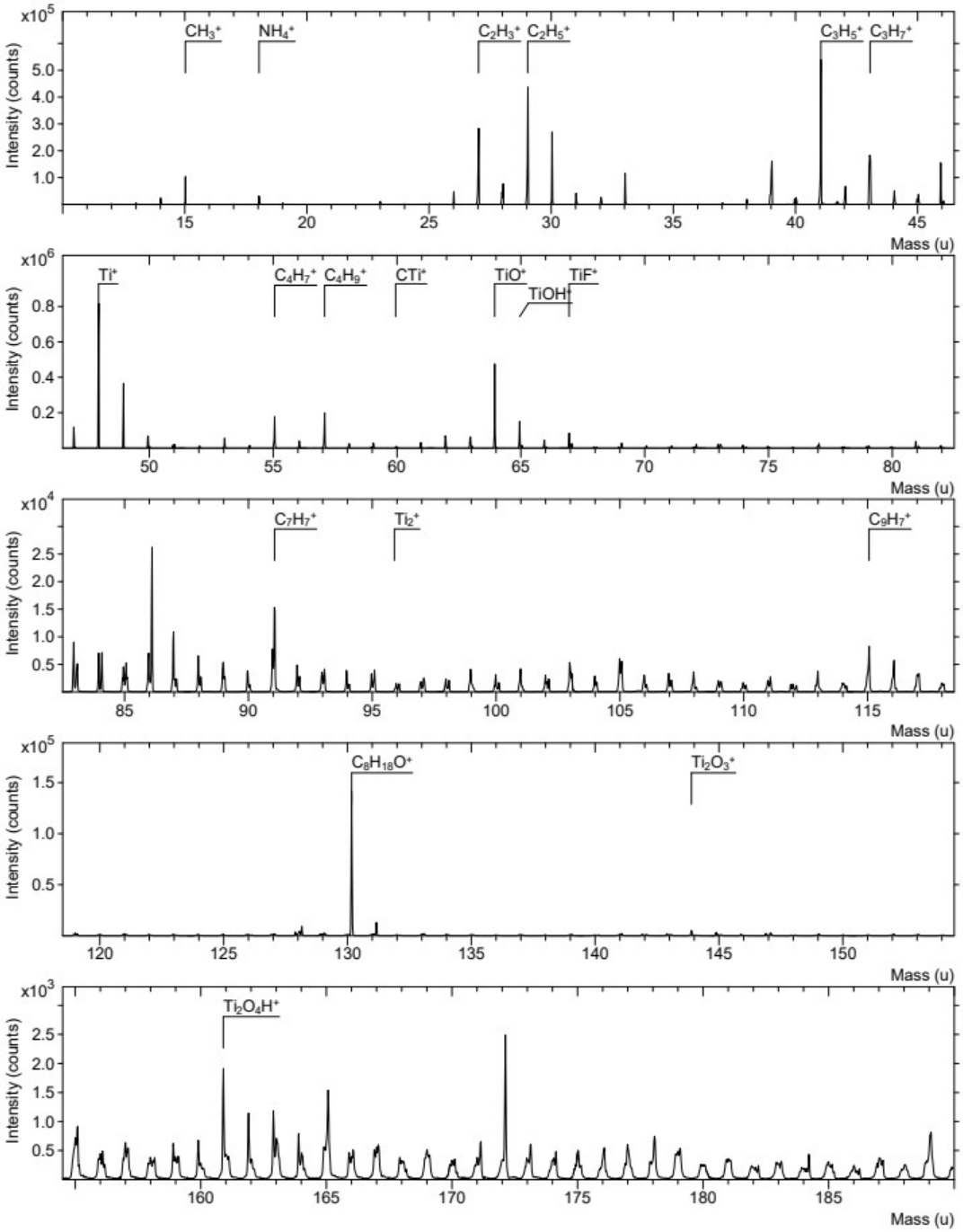

Fig. S4: Mass spectrum of fragments for $Ti_3C_2T_x$ MXene in positive polarity.

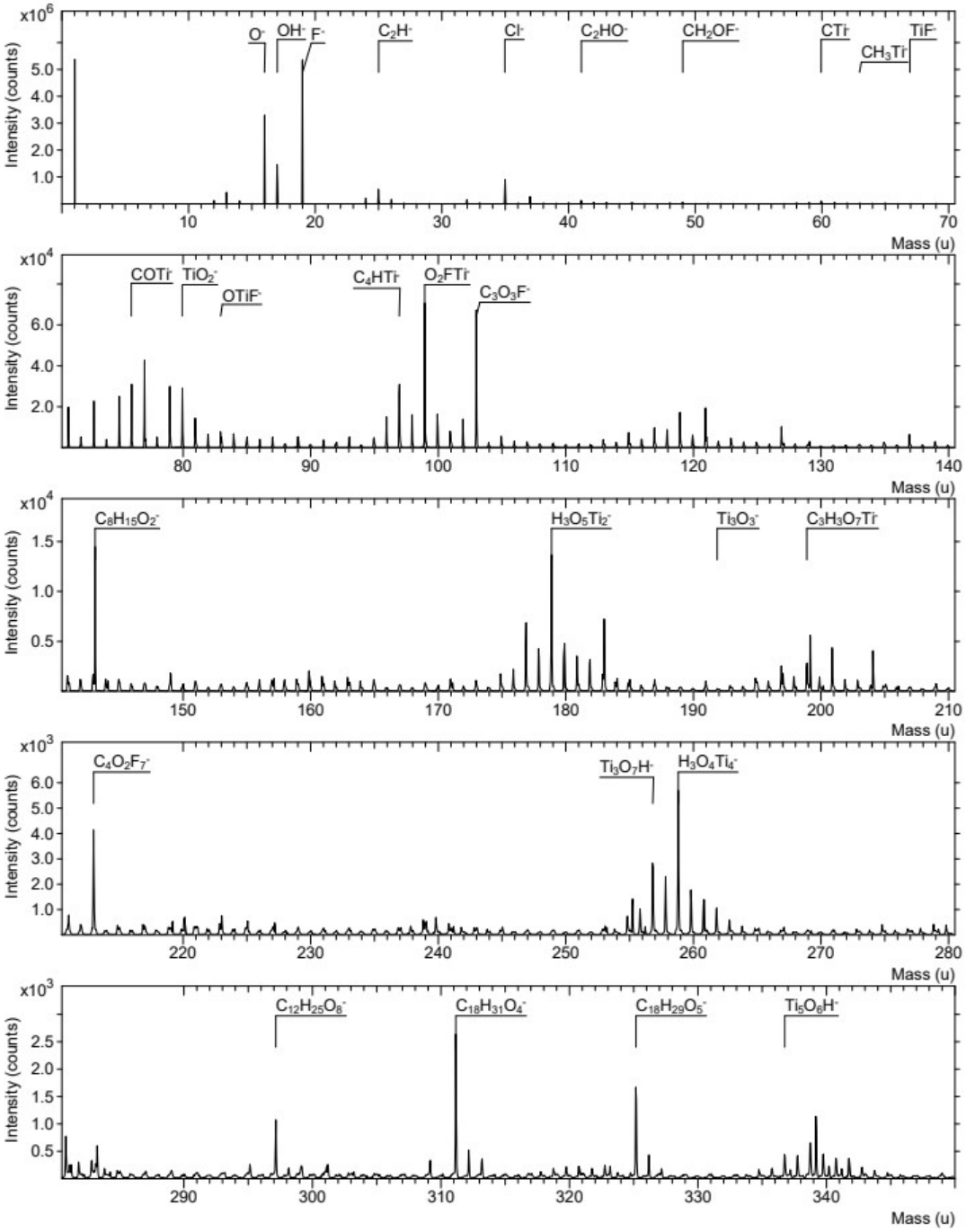

Fig. S5: Mass spectrum of fragments for $Ti_3C_2T_x$ MXene in negative polarity.

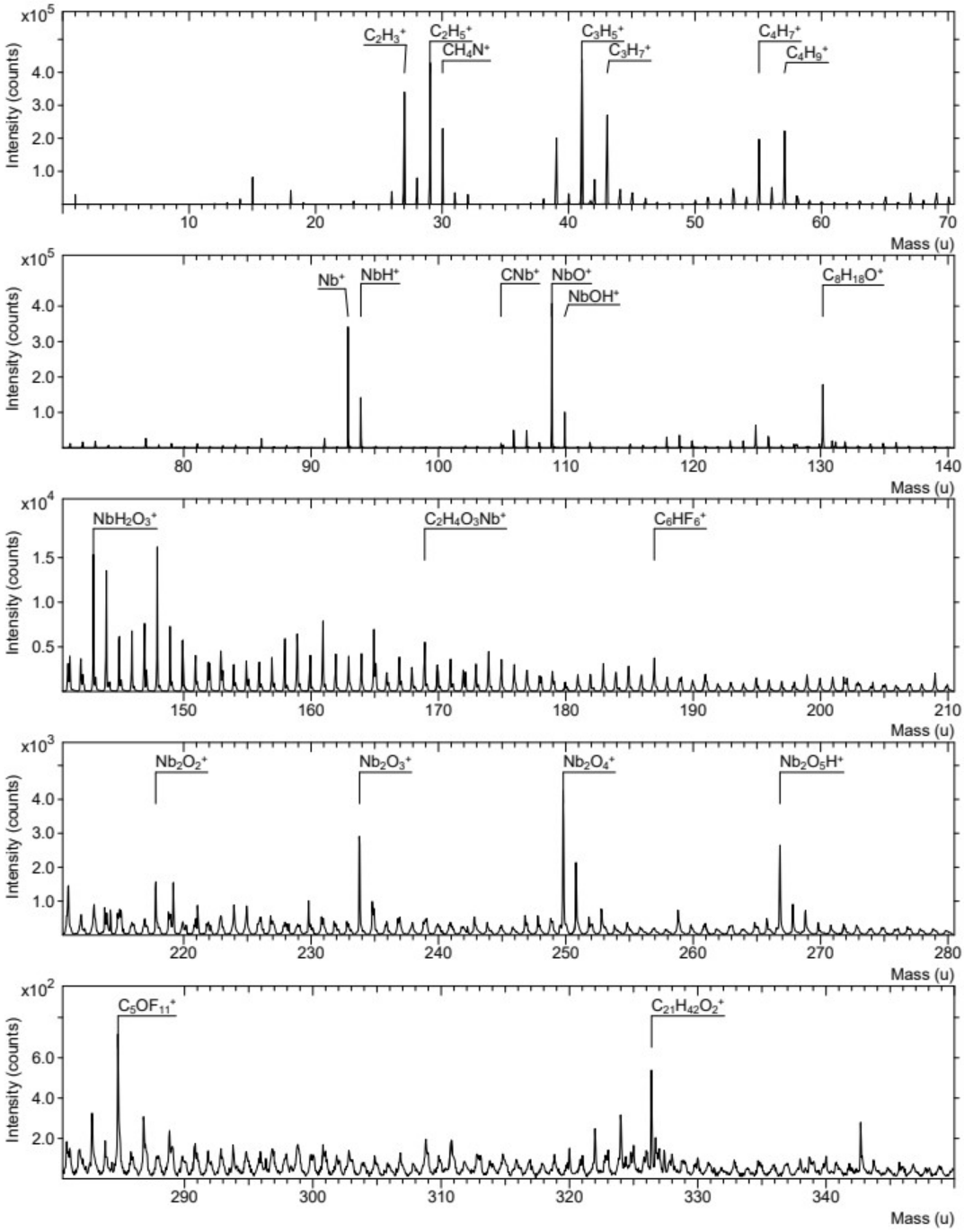

Fig. S6: Mass spectrum of fragments for $Nb_4C_3T_x$ MXene in positive polarity.

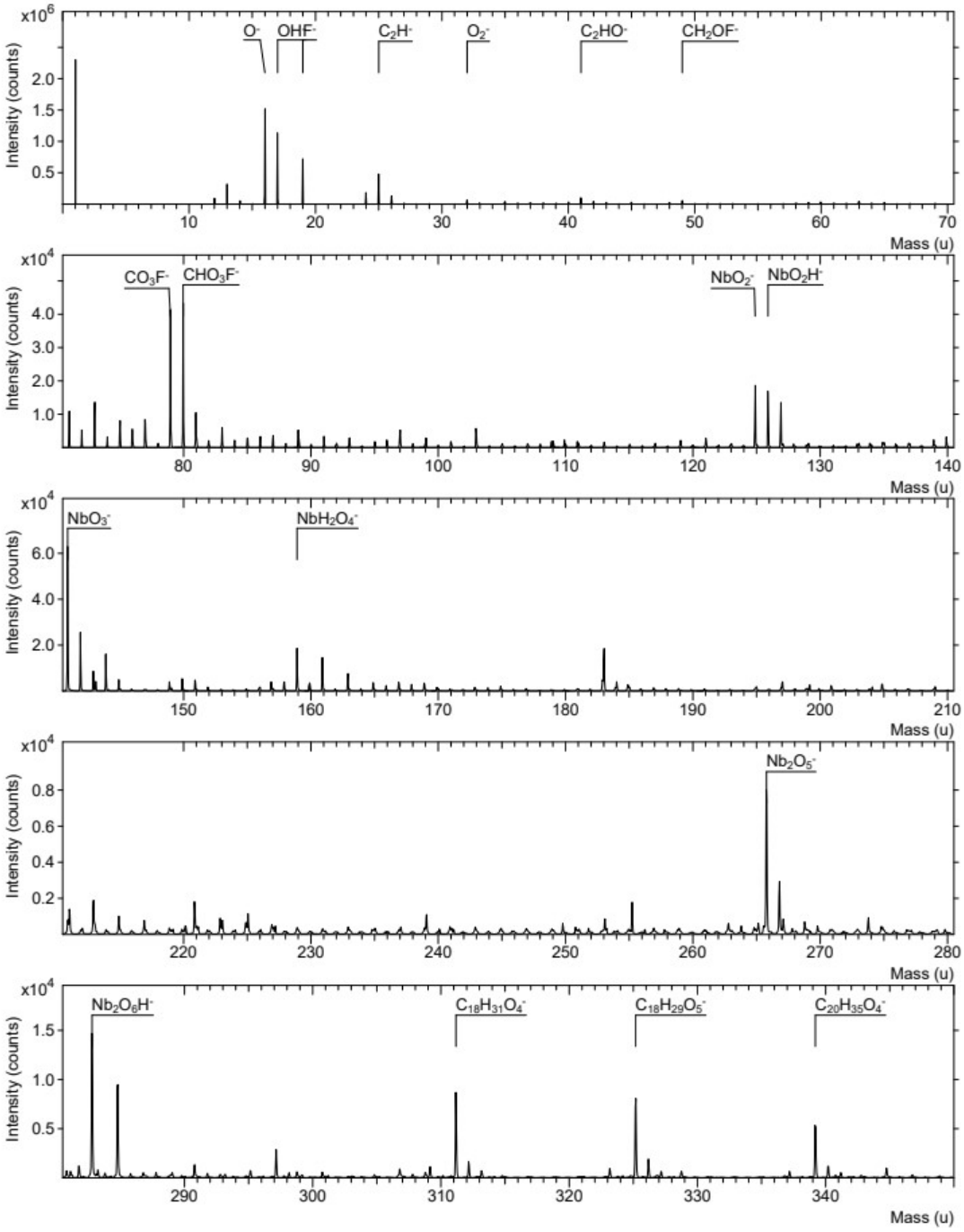

Fig. S7: Mass spectrum of fragments for $Nb_4C_3T_x$ MXene in negative polarity.

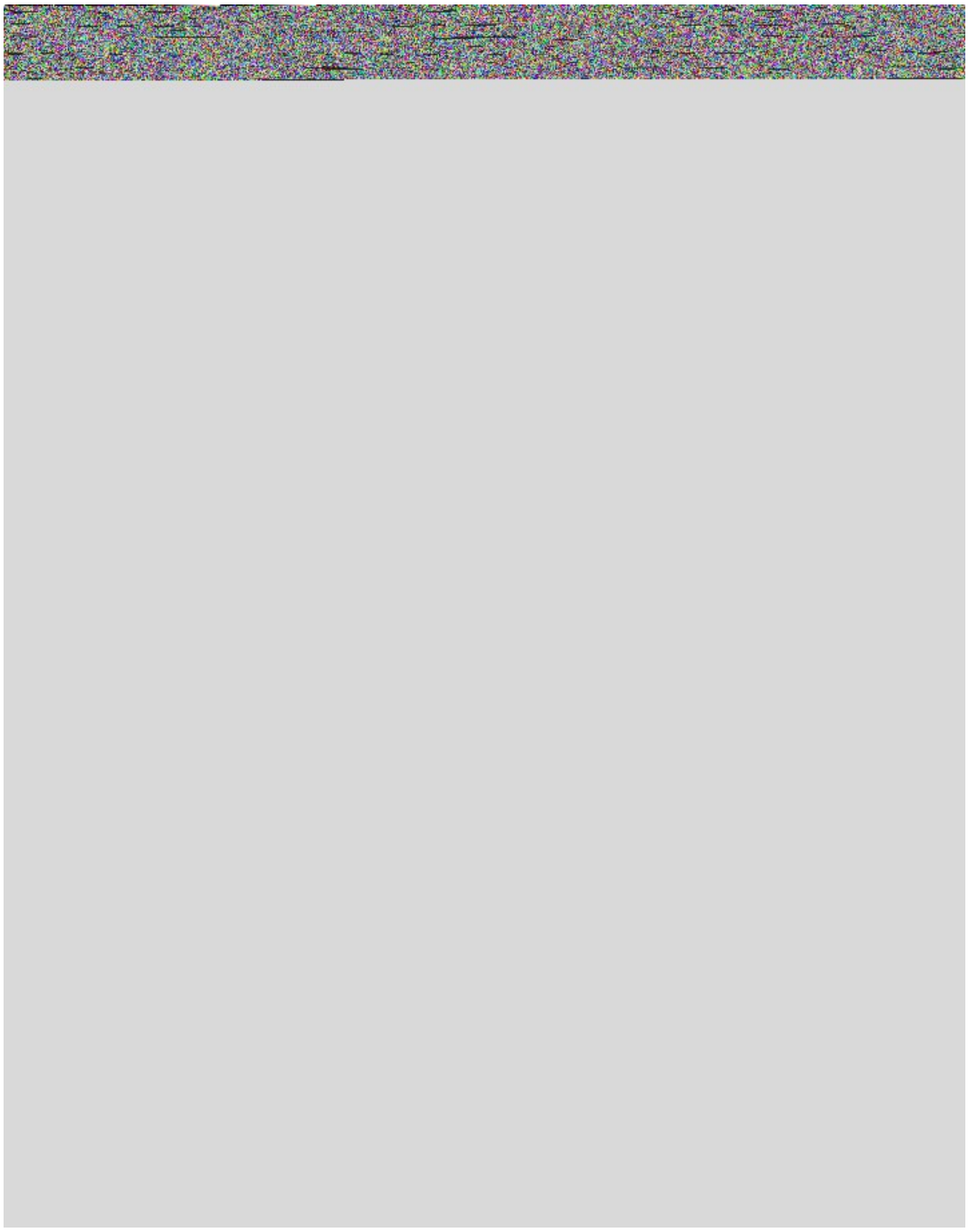

Fig. S8: Mass spectrum of fragments for Nb_2CT_x MXene in positive polarity.

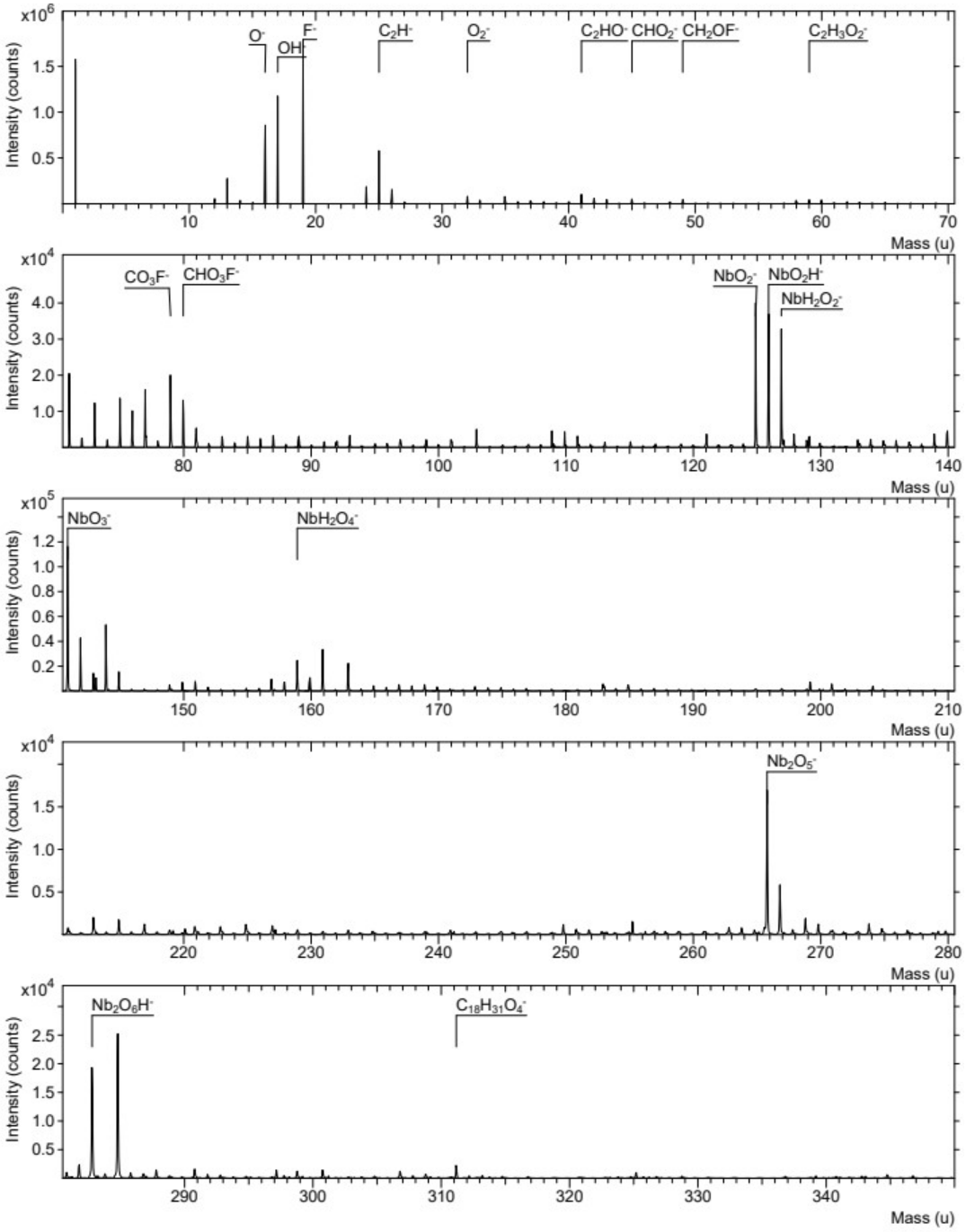

Fig. S9: Mass spectrum of fragments for Nb_2CT_x MXene in negative polarity.

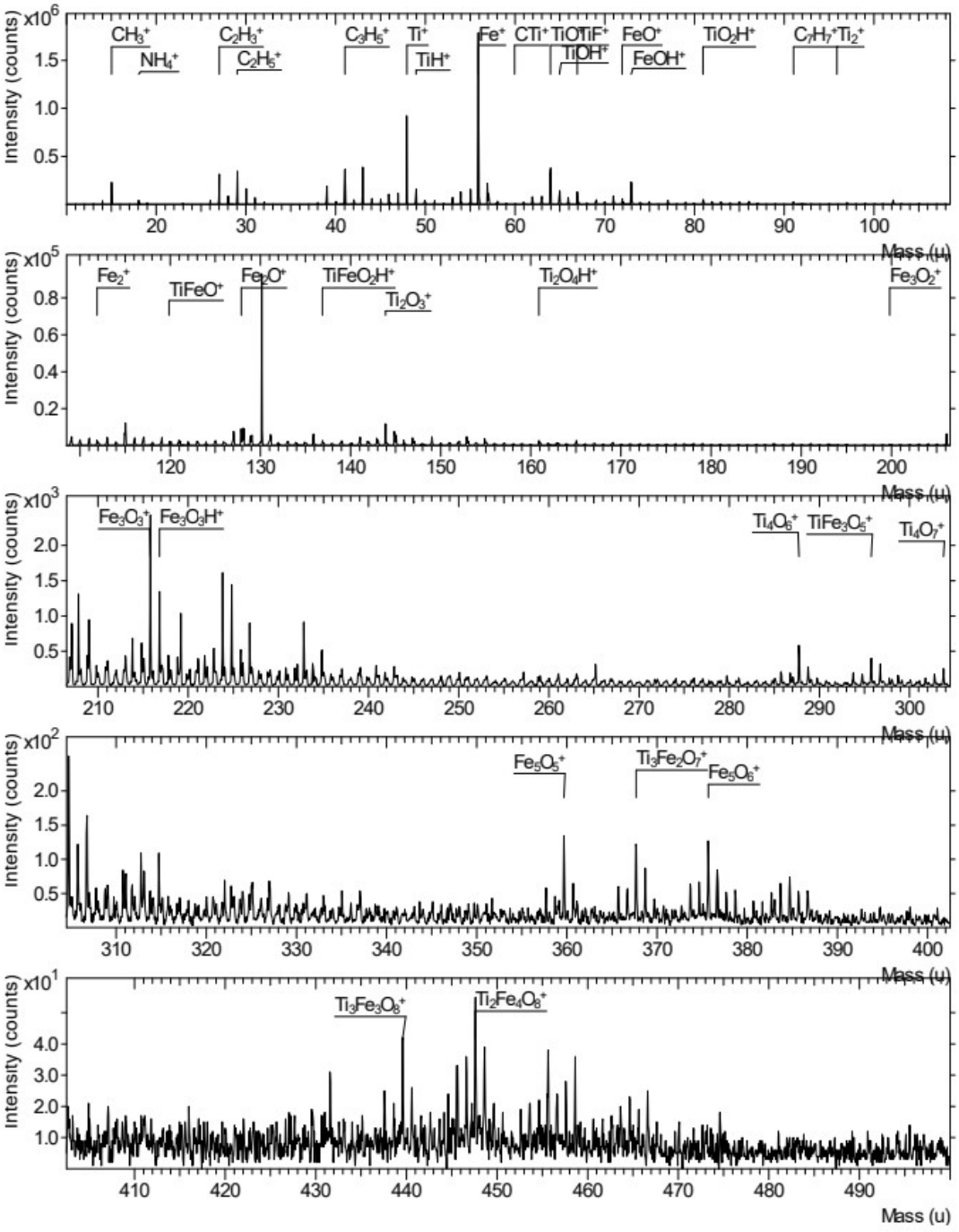

Fig. S10: Mass spectrum of fragments for $Ti_3C_2T_x$@FeNPs in positive polarity.

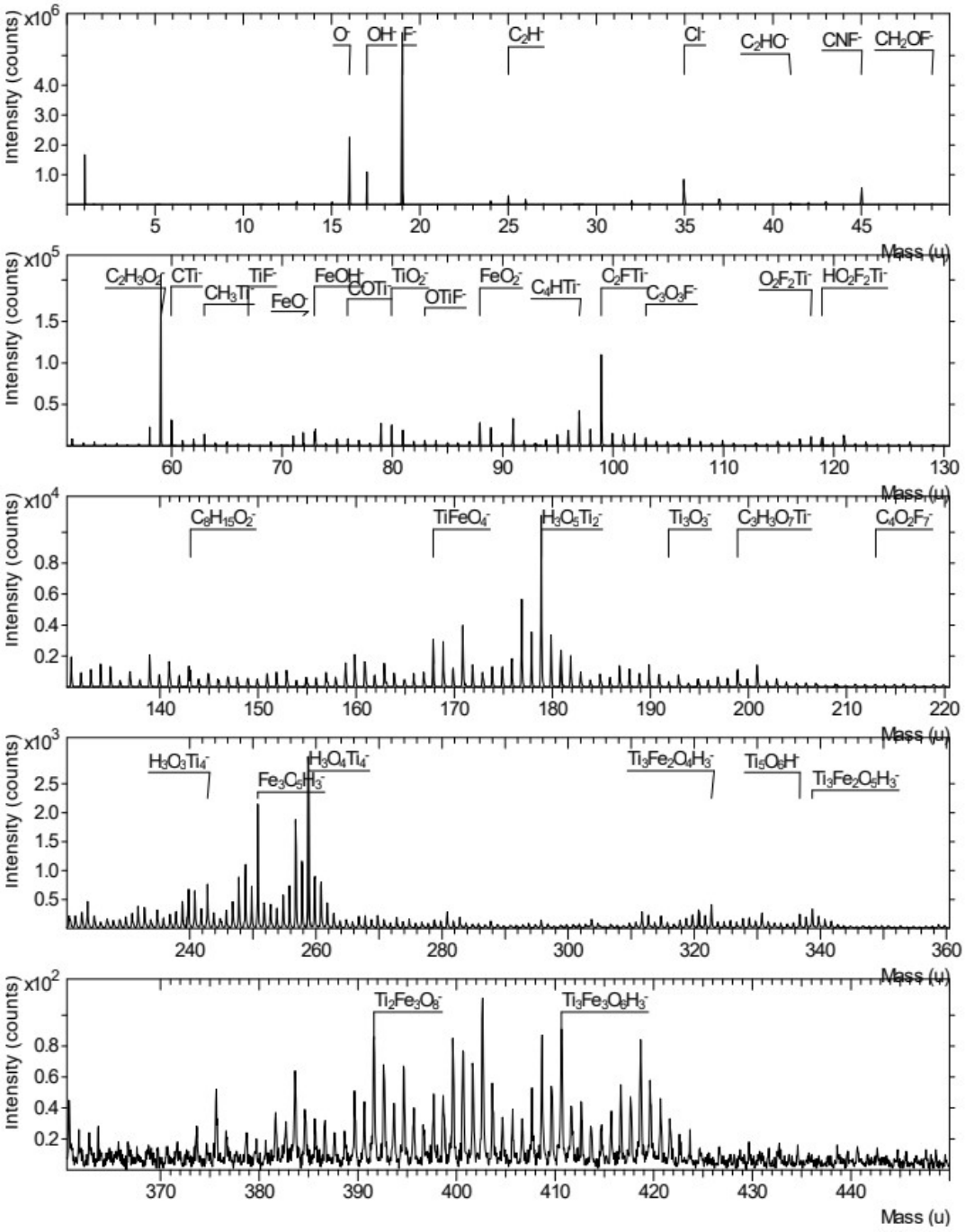

Fig. S11: Mass spectrum of fragments for $Ti_3C_2T_x$@FeNPs in negative polarity.

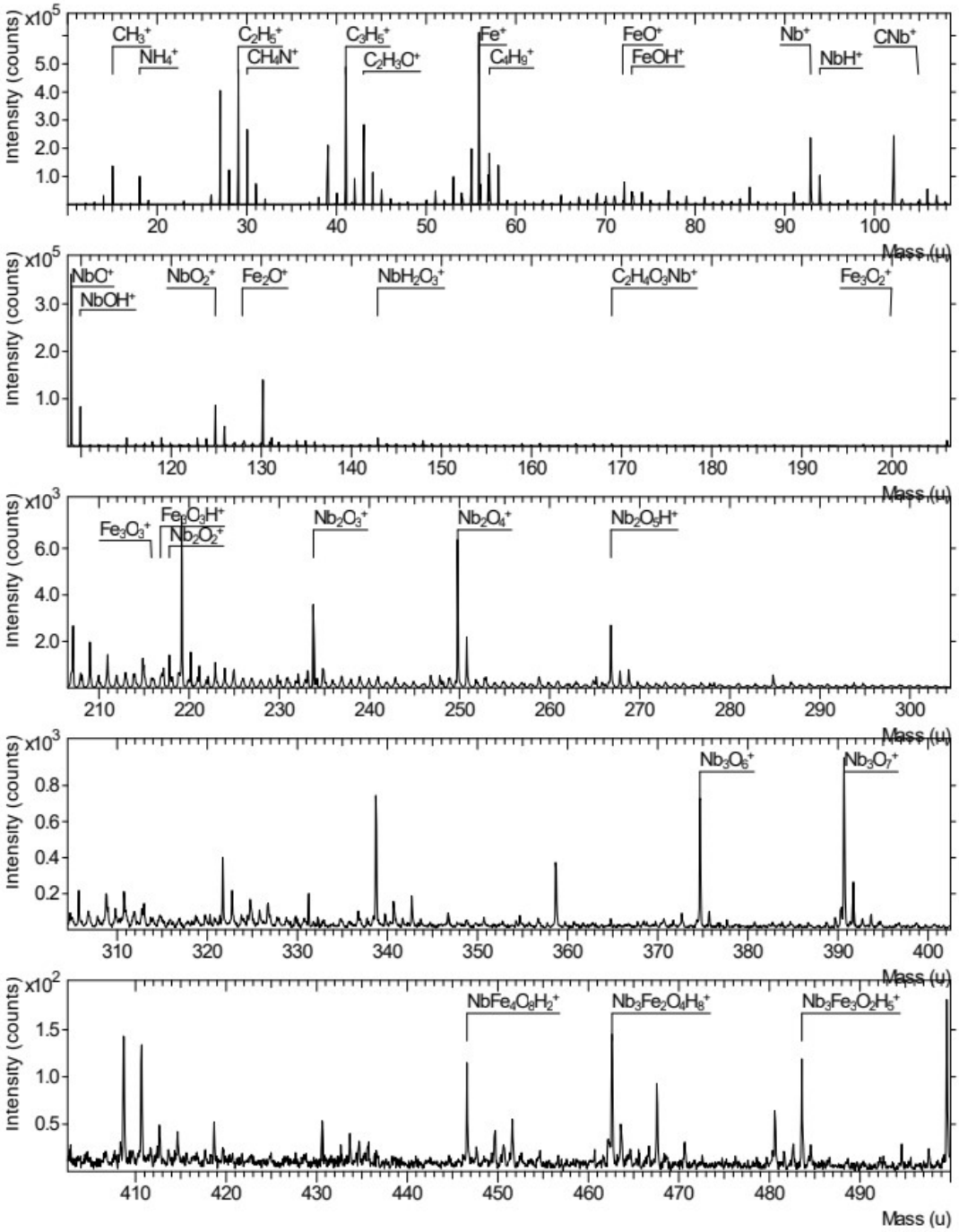

Fig. S12: Mass spectrum of fragments for $Nb_4C_3T_x$@FeNPs in positive polarity.

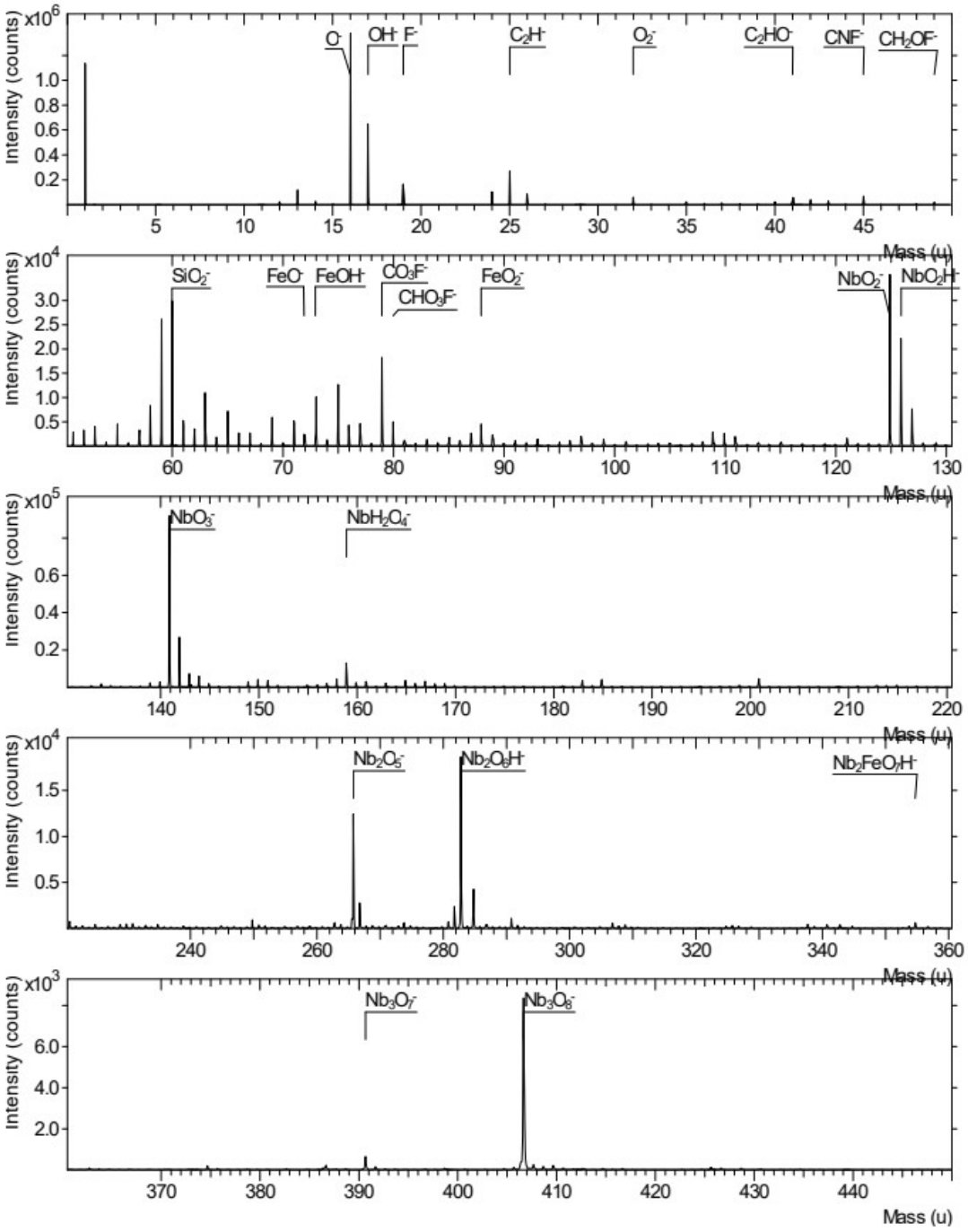

Fig. S13: Mass spectrum of fragments for $Nb_4C_3T_x$@FeNPs in negative polarity.

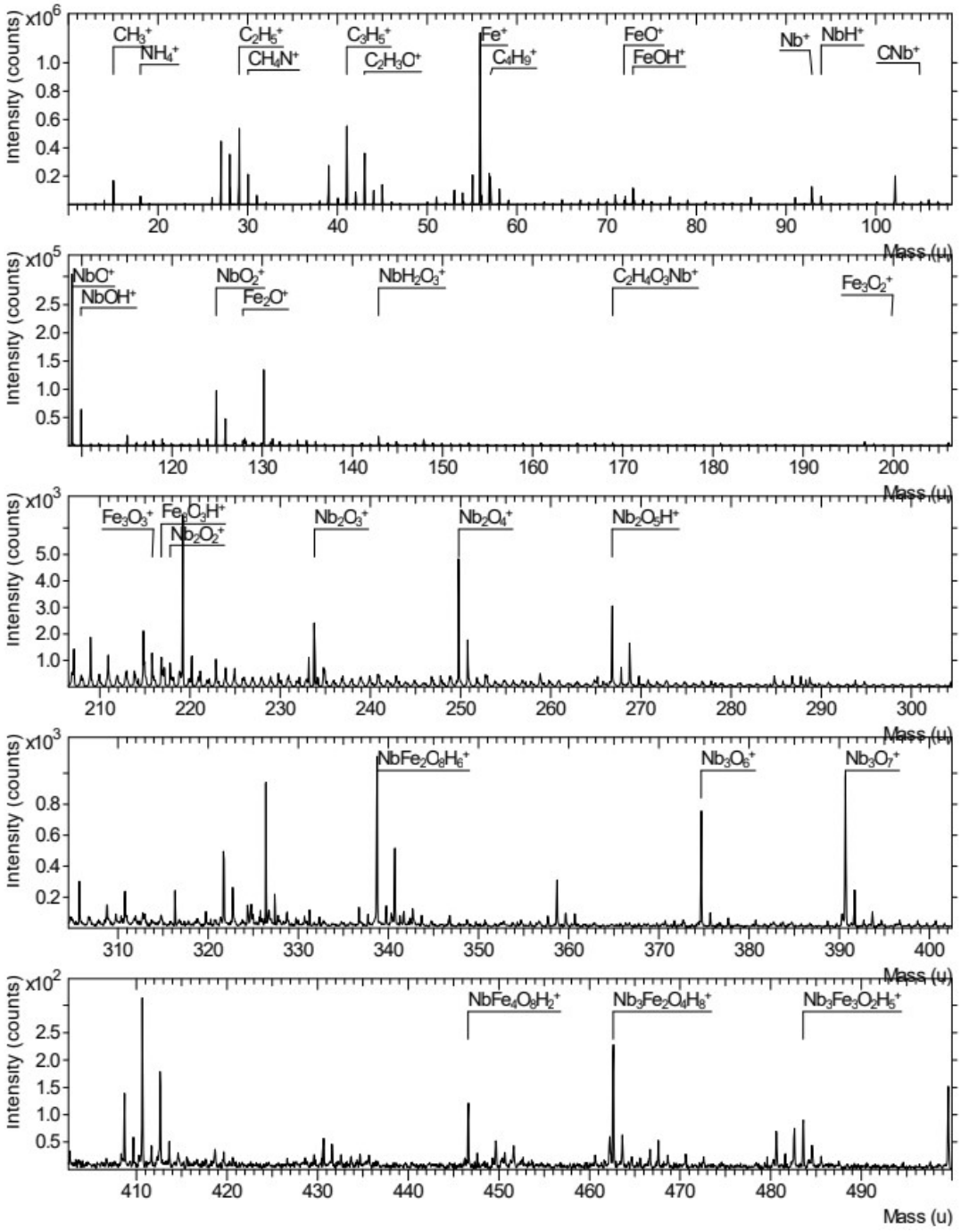

Fig. S14: Mass spectrum of fragments for Nb_2CT_x@FeNPs in positive polarity.

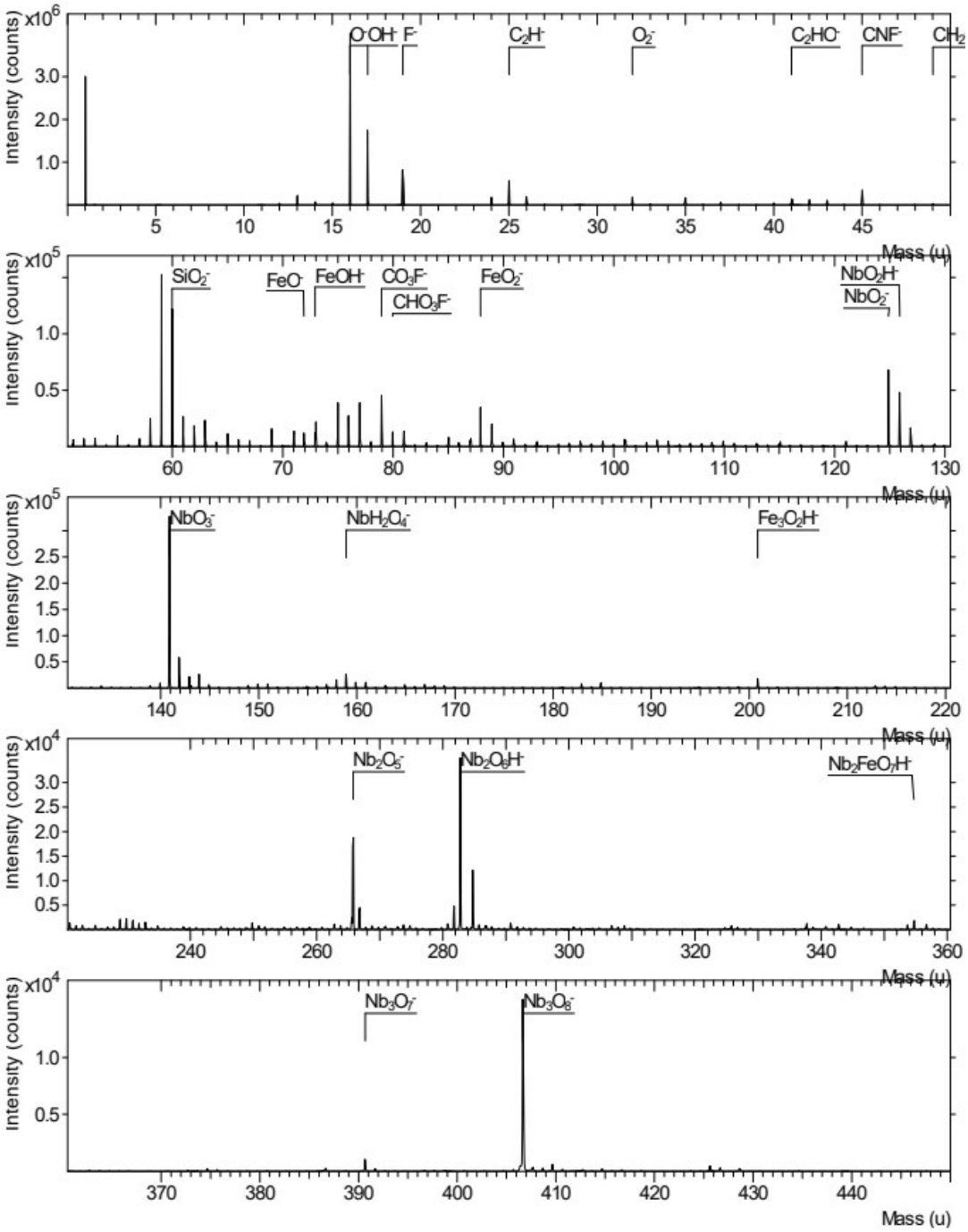

Fig. S15: Mass spectrum of fragments for Nb_2CT_x@FeNPs in negative polarity.

Figure S16 represents the 2D distribution of the selected species in positive polarity: Ti^+, TiO^+, TiF^+, Fe^+, sum of FeO^+, $FeOH^+$, Fe_2O^+, $Fe_3O_2^+$, $Fe_3O_3^+$, $Fe_3O_3H^+$ and $Fe_3O_4H^+$ and sum of $TiFe^+$, $TiFeO^+$, $TiFeO_2$+, $TiFeO_2H^+$ and $Ti_2Fe_3O_2^+$ for $Ti_3C_2T_x$ MXene@FeNPs.

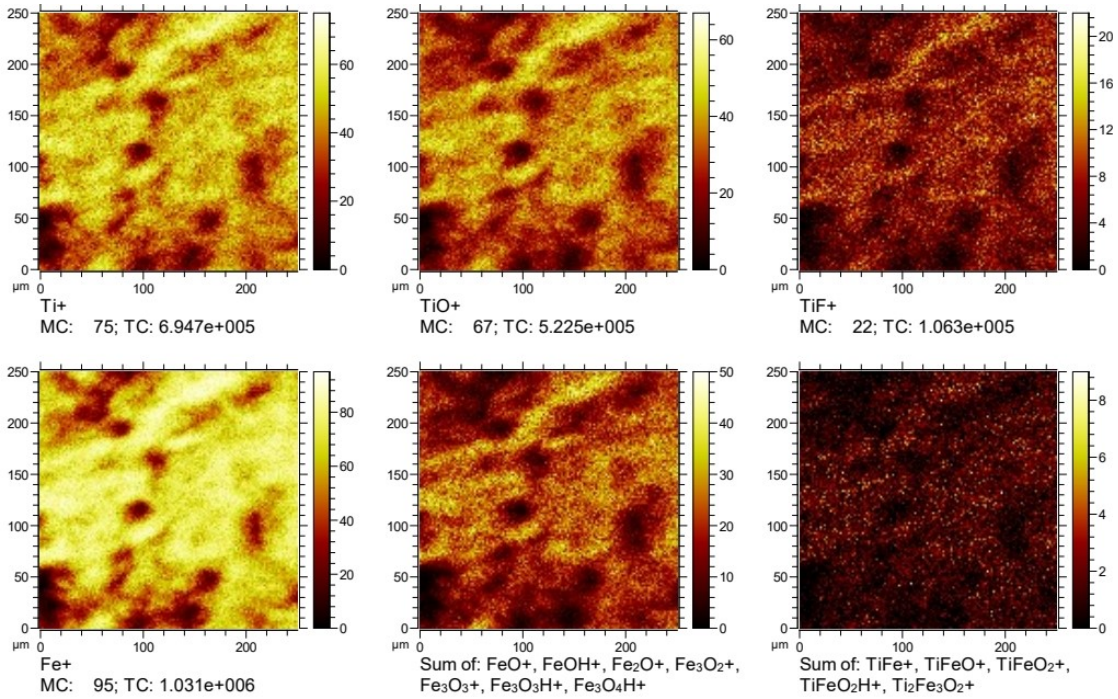

Fig. S16: SIMS 2D distribution for the selected fragments of $Ti_3C_2T_x$@FeNPs in positive polarity.

Figure S17 represents the 2D distribution of the selected species in positive polarity: Nb^+, NbO^+, NbO_2^+, Fe^+, sum of FeO^+, $FeOH^+$ and sum of $NbFeO_2^+$, $Nb_2FeO_6H^+$, $NbFe_4O_8H_2^+$ and $Nb_3Fe_2O_4H_8^+$ for $Nb_4C_3T_x$ MXene@FeNPs.

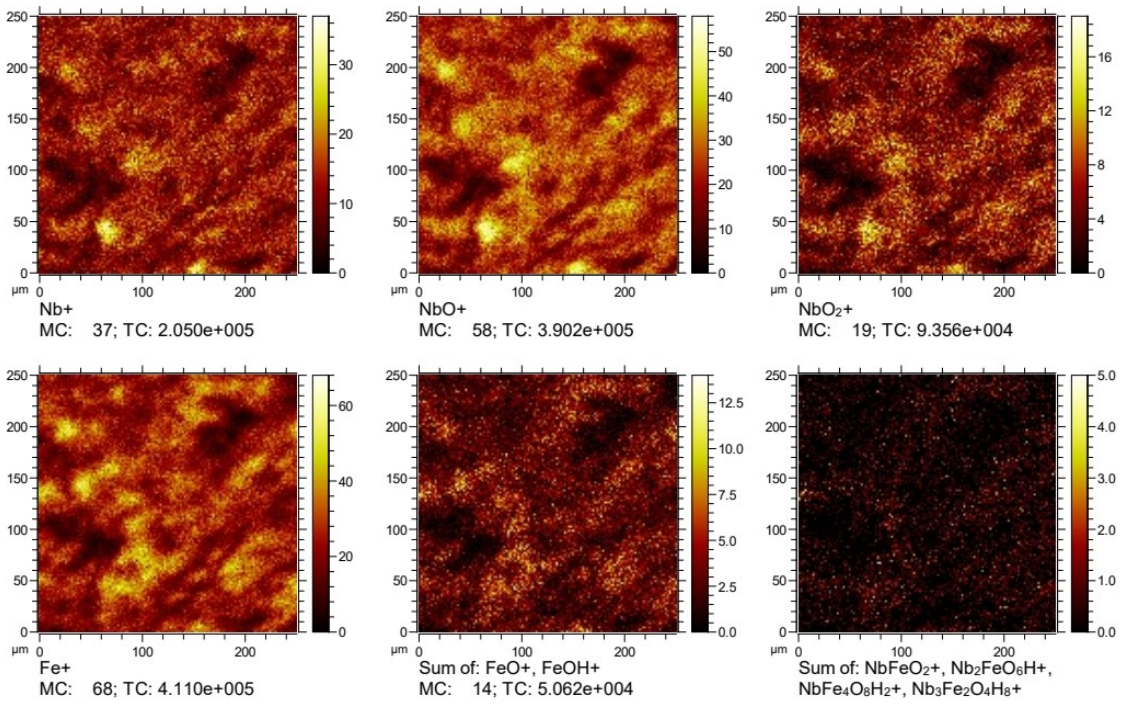

Fig. S17: SIMS 2D distribution for the selected fragments of $Nb_4C_3T_x$@FeNPs in positive polarity.

Figure S18 represents the 2D distribution of the selected species in positive polarity: Nb^+, NbO^+, NbO_2^+, Fe^+, sum of FeO^+, $FeOH^+$, $Fe_3O_2^+$ and sum of $NbFeO_2^+$, $Nb_2FeO_6H^+$, $NbFe_4O_8H_2^+$ and $Nb_3Fe_2O_4H_8^+$ for Nb_2CT_x MXene@FeNPs.

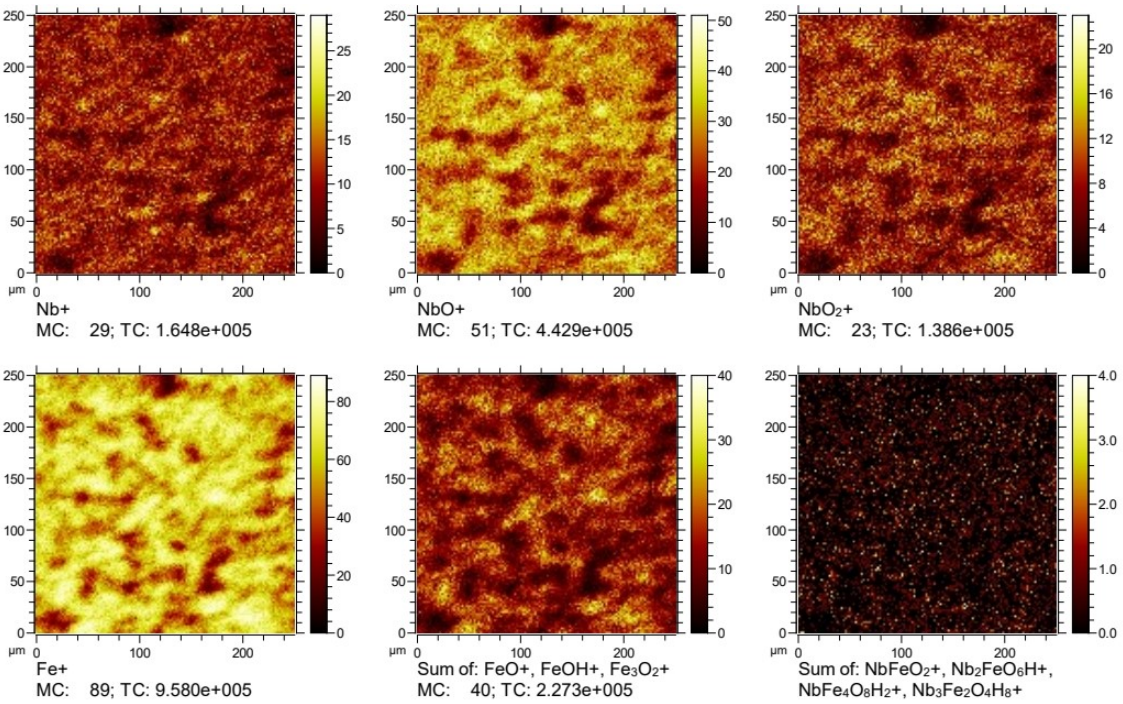

Fig. S18: SIMS 2D distribution of the selected fragments for Nb_2CT_x@FeNPs in positive polarity.

Figure S19 represents the 2D distribution of the selected species in negative polarity: OH^-, TiO^-, TiO_2^-, sum of FeO^-, FeO_2^-, $Fe_3O_4^-$ and $Fe_4O_6^-$ and sum of $TiFeO_4^-$ and $Ti_2Fe_3O_8^-$ for $Ti_3C_2T_x$ MXene@FeNPs.

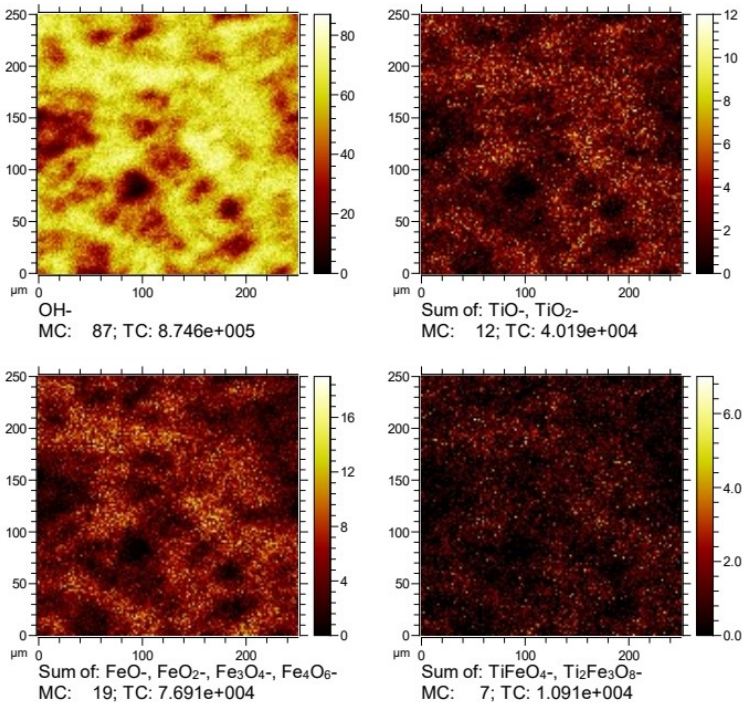

Fig. S19: SIMS 2D distribution for the selected fragments of $Ti_3C_2T_x$@FeNPs in negative polarity.

Figure S20 represents the 2D distribution of the selected species in negative polarity: OH^-, sum of NbO^-, NbO_2^-, NbO_2H^- and NbO_3^-, sum of FeO^-, FeO_2^-, $FeOH^-$ and sum of $Nb_2FeO_7H^-$ and $Nb_4FeO_3H_3^-$ for $Nb_4C_3T_x$ MXene@FeNPs.

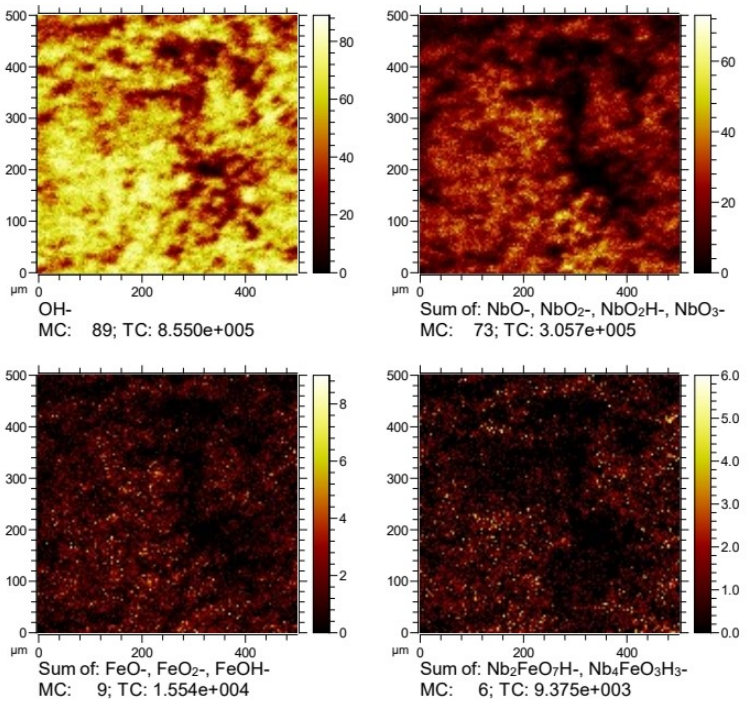

Fig. S20: SIMS 2D distribution for the selected fragments of $Nb_4C_3T_x$@FeNPs in negative polarity.

Figure S21 represents the 2D distribution of the selected species in negative polarity: OH^-, sum of NbO^-, NbO_2^- and NbO_3^-, sum of FeO^-, $FeOH^-$, FeO_2^- and $Fe_3O_4^-$ and sum of $Nb_2FeO_7H^-$ and $Nb_4FeO_3H_3^-$ for Nb_2CT_x MXene@FeNPs.

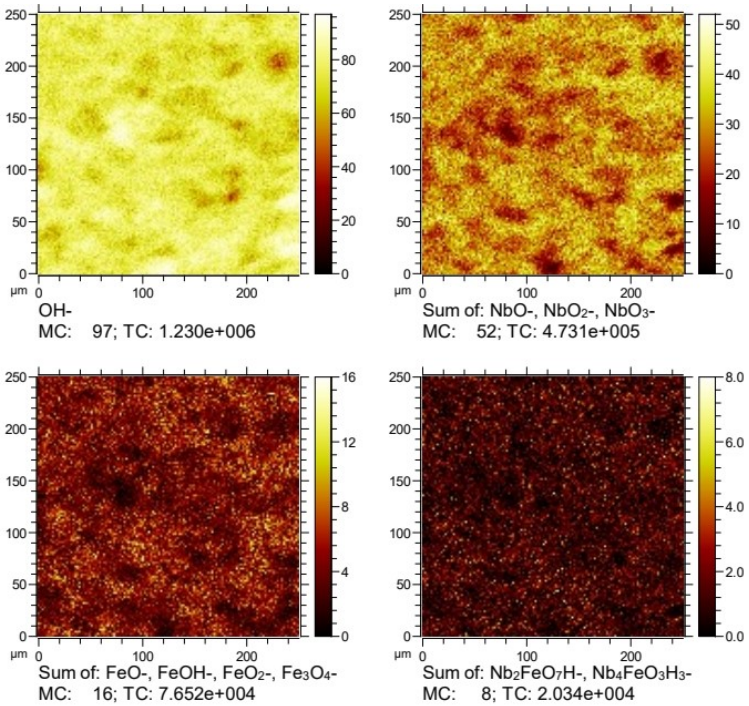

Fig. S21: SIMS 2D distribution for the selected fragments of Nb_2CT_x@FeNPs in negative polarity.

Table S1: The values of normalized intensities for identified ions in $Ti_3C_2T_x$, $Nb_4C_3T_x$ and Nb_2CT_x MXenes with iron oxide nanoparticles in positive and negative polarity.

Ion	Mass / m. u.	$Ti_3C_2T_x$	$Nb_4C_3T_x$	Nb_2CT_x
Fe^+	55.93	1.59×10^{-1}	6.05×10^{-2}	1.16×10^{-1}
FeO^+	71.93	3.91×10^{-3}	8.69×10^{-4}	1.99×10^{-3}
$FeOH^+$	72.94	1.97×10^{-2}	4.43×10^{-3}	1.10×10^{-2}
Fe_2^+	111.87	3.67×10^{-4}	9.96×10^{-5}	2.66×10^{-4}
$TiFe^+$	103.88	7.45×10^{-5}	-	-
$TiFeO^+$	119.88	1.89×10^{-4}	-	-
$TiFeO_2^+$	135.88	9.75×10^{-4}	-	-
$TiFeO_2H^+$	136.88	3.31×10^{-4}	-	-
Fe_2O^+	127.87	1.46×10^{-3}	2.92×10^{-4}	8.74×10^{-4}
$Fe_3O_2^+$	199.80	7.30×10^{-5}	6.13×10^{-5}	1.06×10^{-4}
$Fe_3O_3^+$	215.81	3.22×10^{-4}	8.29×10^{-5}	2.08×10^{-4}
$Fe_3O_3H^+$	216.81	1.64×10^{-4}	7.23×10^{-5}	1.67×10^{-4}
$Ti_2Fe_3O_2^+$	295.75	7.83×10^{-5}	-	-
$Ti_2Fe_4O_3^+$	367.67	3.13×10^{-5}	-	-
$Ti_3Fe_3O_4^+$	375.68	3.41×10^{-5}	-	-
$Ti_2Fe_4O_8^+$	447.62	1.90×10^{-5}	-	-
FeO^-	71.92	1.62×10^{-3}	6.56×10^{-4}	1.59×10^{-3}
$FeOH^-$	72.93	1.77×10^{-3}	5.87×10^{-4}	1.71×10^{-3}
FeO_2^-	87.92	5.39×10^{-3}	1.13×10^{-3}	3.75×10^{-3}
$TiFeO_4^-$	167.87	5.71×10^{-4}	-	-
$Fe_3O_5H_3^-$	250.80	3.81×10^{-5}	-	-
$Ti_3Fe_2O_4H_3^-$	322.73	5.43×10^{-5}	-	-
$Ti_2Fe_3O_8^-$	391.64	3.32×10^{-5}	-	-
$Ti_3Fe_3O_6H_3^-$	410.65	3.70×10^{-5}	-	-
$Fe_3O_4^-$	231.79	6.10×10^{-5}	8.62×10^{-5}	1.92×10^{-4}
$Fe_2O_3^-$	159.88	4.89×10^{-4}	2.37×10^{-4}	1.82×10^{-4}
$Fe_4O_6^-$	319.74	5.83×10^{-5}	-	-
$NbFe^+$	148.84	-	5.71×10^{-5}	5.93×10^{-5}

$NbFeO^+$	164.83	-	1.80×10^{-4}	1.97×10^{-4}
$NbFeO_2^+$	180.83	-	3.1×10^{-4}	4.21×10^{-4}
$NbFeO_2H^+$	181.84	-	1.40×10^{-4}	1.85×10^{-4}
$Nb_2FeO_6H^+$	338.73	-	1.77×10^{-4}	2.10×10^{-4}
$NbFe_4O_8H_2^+$	446.60	-	1.96×10^{-5}	1.89×10^{-5}
$Nb_3Fe_2O_4H_8^+$	462.63	-	4.36×10^{-5}	4.98×10^{-5}
$Fe_3O_2H^-$	200.88	3.51×10^{-3}	2.01×10^{-3}	1.58×10^{-3}
$Nb_2FeO_7H^-$	354.72	-	2.54×10^{-4}	3.67×10^{-4}
$Nb_4FeO_3H_3^-$	478.60	-	6.60×10^{-4}	8.06×10^{-4}

Table S2: The values of normalized intensities for identified ions in $Ti_3C_2T_x$, $Nb_4C_3T_x$ and Nb_2CT_x MXenes with iron oxide nanoparticles in negative polarity.

Sample	F^-	OH^-
$Ti_3C_2T_x$	2.25×10^{-1}	9.9×10^{-2}
$Nb_4C_3T_x$	6.8×10^{-2}	1.07×10^{-1}
Nb_2CT_x	1.21×10^{-1}	9.74×10^{-2}
$Ti_3C_2T_x$@FeNPs	3.39×10^{-1}	6.1×10^{-2}
$Nb_4C_3T_x$@FeNPs	3.86×10^{-2}	0.82×10^{-1}
Nb_2CT_x@FeNPs	2.65×10^{-2}	6.91×10^{-2}

Table S3: The values of normalized intensities ratios of oxygen and fluorine ions in three types of MXenes with and without Fe oxides nanoparticles in negative polarity.

Ratios	**$Ti_3C_2T_x$**	**$Nb_4C_3T_x$**	**Nb_2CT_x**
O:F	0.62	2.17	0.97
O:F with Fe NP	0.45	4.58	3.78
OH:F	0.44	1.55	0.81
OH:F with Fe NP	0.17	2.41	1.95

Optical Faraday effect in reference samples

In order to evaluate our experimental setup (**Fig. S20**), we ran a set of tests on reference samples.

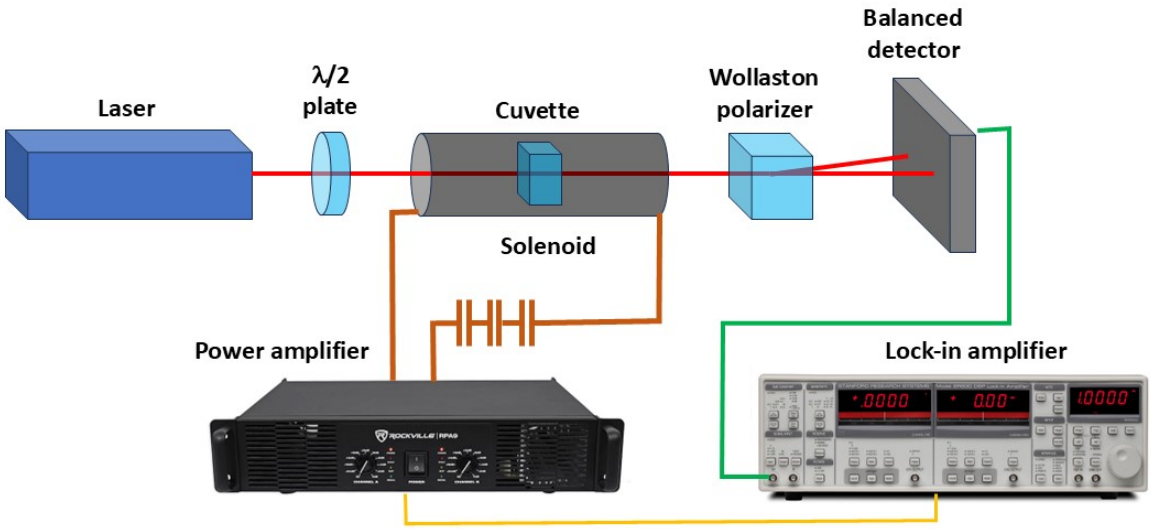

Fig. S22: OFE experimental setup.

We started by checking the Faraday response of pure water. As can be see in **Fig. S23** water shows a strong and clean linear response up to the highest applied field of 5 mT. This is expected as water is well known to be a strong diamagnetic medium under our conditions [1].

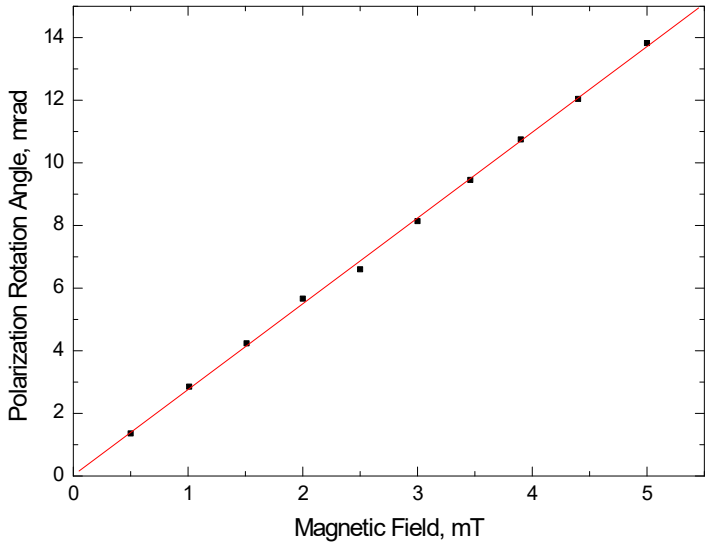

Fig. S23: Faraday response of pure water.

Next we have investigated our LAL prepared NP samples. Unlike the samples containing MXenes as given in the main text, pure NP solutions did not show excessive scattering and hence no shaking was needed between individual measurements. **Figure S24** shows Faraday response of the solutions containing 300 µg of the NPs *per* mL of water at the fundamental and third harmonic frequency. The data is well fitted by the model introduced earlier by Patterson *et al*. [2] thereby confirming the superparamagnetic nature of our as prepared NPs.

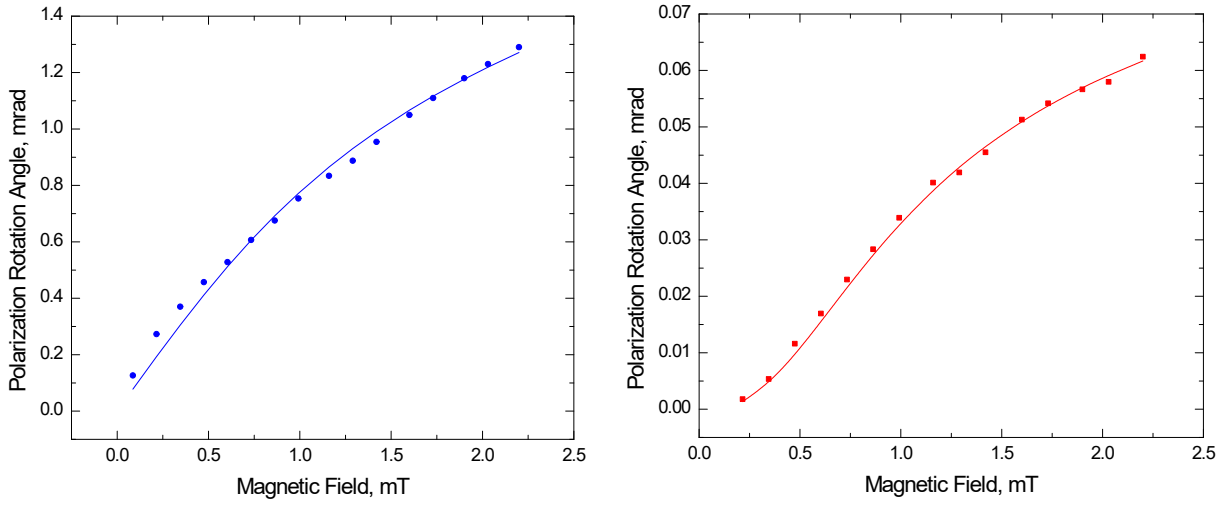

Fig. S24: Faraday response of the LAL prepared FeNPs dissolved in water at the fundamental (153 Hz) and third harmonic frequency (459 Hz).

References

[1] F. Gutiérrez-Mejía, J.C. Ruiz-Suárez, „AC magnetic susceptibility at medium frequencies suggests a paramagnetic behavior of pure water,“ Journal of Magnetism and Magnetic Materials Volume 324, Issue 6, March 2012, Pages 1129-1132.

[2] C. Patterson, M. Syed, Y. Takemura, Harmonic decomposition of magneto-optical signal from suspensions of superparamagnetic nanoparticles, Journal of Magnetism and Magnetic Materials, 451 (2018) 248-253.